JPE 16-6-24

http://dx.doi.org/10.6113/JPE.2016.16.6.2231
ISSN(Print): 1598-2092 / ISSN(Online): 2093-4718

Simplified Model Predictive Control Method for Three-Phase Four-Leg Voltage Source Inverters

Soo-eon Kim*, So-Young Park*, and Sangshin Kwak†

*,†School of Electrical and Electronics Engineering, Chung-ang University, Seoul, Korea

Abstract

A simplified model predictive control method is presented in this paper. This method is based on a future reference voltage vector for a three-phase four-leg voltage source inverter (VSI). Compared with the three-leg VSIs, the four-leg VSI increases the possible switching states from 8 to 16 owing to a fourth leg. Among the possible states, this should be considered in the model predictive control method for selecting an optimal state. The increased number of candidate switching states and the corresponding voltage vectors increase the calculation burden. The proposed technique can preselect 5 among the 16 possible voltage vectors produced by the three-phase four-leg voltage source inverters, based on the position of the future reference voltage vector. The discrete-time model of the future reference voltage vector is built to predict the future movement of the load currents, and its position is used to choose five preselected vectors at every sampling period. As a result, the proposed method can reduce calculation load by decreasing the candidate voltage vectors used in the cost function for the four-leg VSIs, while exhibiting the same performance as the conventional method. The effectiveness of the proposed method is demonstrated with simulation and experiment results.

Key words: Current control, Model predictive control, Three-phase four-leg voltage source inverter

I. INTRODUCTION

Three-phase four-leg voltage source inverters (VSIs) can provide output voltages and current waveforms with improved quality. Compared with the three-phase three-leg VSIs, the additional fourth leg, which is connected to the neutral point of the load, increases the switching states from 8 to 16. Traditional current control methods for the four-leg VSIs employ the proportional-integral (PI) regulator along with the pulse width modulation (PWM) stages. The carrier-based sinusoidal PWM method [1]-[6] and 3-D space vector modulation [7]-[10] have been widely used for four-leg VSIs. With the development of high-performance microprocessors, the model predictive control method [11]-[17] has been recently developed as a simple and effective current control method. This is because the method does not require the design of the internal current control loops, the gain regulation of the PI controllers, and the use of individual PWM blocks. In addition, the model predictive control method can provide advantages such as a fast dynamic response, an inherent decoupling, and a simple inclusion of multiple objectives. As the model predictive control method selects one optimal state after considering all the possible switching states produced by a converter, the increase in the switching states of the four-leg VSIs from 8 to 16 increase the candidate switching states in the control method, thereby increasing calculation burden.

This paper presented a simplified model predictive control method based on a future reference voltage vector for a three-phase four-leg VSI. The proposed technique can preselect 5 among the 16 possible voltage vectors produced by the three-phase four-leg voltage source inverter. This is based on the position of the future reference voltage vector. The discrete-time model of the future reference voltage vector is established to predict the future movement of the load currents, and its position is used to choose five preselected vectors at every sampling period. As a result, the proposed method can reduce the calculation load by decreasing the number of candidate voltage vectors used in the cost function for the four-leg VSIs, while exhibiting the same performance as the conventional method. The effectiveness of the

Manuscript received Mar. 30, 2016; accepted Jul. 25, 2016
Recommended for publication by Associate Editor Yong Kang.
†Corresponding Author: sskwak@cau.ac.kr
Tel: +82-2-820-5346, Fax: +82-2-825-1584, Chung-ang University
*School of Electrical and Electronics Eng., Chung-ang University, Korea

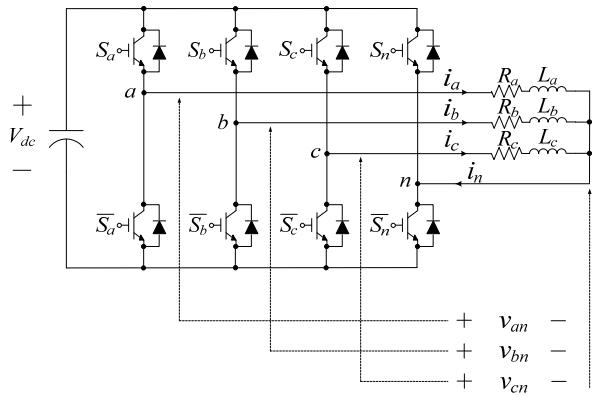

Fig. 1. Three-phase two-level four-leg inverter topology.

proposed method is demonstrated with simulation and experimental results.

II. Conventional Model Predictive Current Control Method for Three-Phase Four-Leg VSIs

A three-phase four-leg VSI with four legs and a general three-phase resistive-inductive (*RL*) load is shown in Fig. 1. Compared with a three-leg VSI, the fourth leg of the four-leg VSI connects to the neutral point of the load. The upper and lower switches in the same leg work with a complementary operation. Thus, the output phase voltages of the four-leg VSI are determined depending on the switching states of the upper switches, S_a, S_b, S_c, and S_n. Each upper switch assumes a binary value of "1" and "0" in the closed and open states, respectively, and 16 switching states are generated by the four-leg VSI.

In the conventional model predictive control method of the four-leg VSI, the future current movements at the $(k+1)^{th}$ step according to the 16 possible switching states are predicted using the mathematical model of the future current. Based on the future current prediction, one optimal switching state is selected through a cost function that minimizes the load current error between the future reference and predicted currents. For simplicity, the three-phase output voltages and currents are represented as vectors:

$$\begin{aligned} \boldsymbol{v} &= \begin{bmatrix} v_{an} & v_{bn} & v_{cn} \end{bmatrix}^{\mathrm{T}} \\ \boldsymbol{i} &= \begin{bmatrix} i_a & i_b & i_c \end{bmatrix}^{\mathrm{T}} \end{aligned} \tag{1}$$

The load current dynamics of the four-leg VSI in Fig. 1 is described as,

$$L\frac{d\boldsymbol{i}}{dt} = \boldsymbol{v} - R\boldsymbol{i} \tag{2}$$

where R and L are the load resistance and inductance, respectively. The derivative of the load current with respect to time in (2) can be approximated in the discrete-time domain as,

$$\frac{d\boldsymbol{i}}{dt} \approx \frac{\boldsymbol{i}(k+1) - \boldsymbol{i}(k)}{T_s} \tag{3}$$

As a result, the one-step future load current can be expressed in the discrete-time form as,

$$\boldsymbol{i}(k+1) = \boldsymbol{i}(k) + \frac{T_s}{L}\left[\boldsymbol{v}(k) - R\boldsymbol{i}(k)\right] \tag{4}$$

The future reference current at the $(k+1)^{th}$ step, for a requirement of the load current control method, can be obtained using the fourth-order Lagrange extrapolation formula as [14],

$$\boldsymbol{i}^*(k+1) = 4\boldsymbol{i}^*(k) - 6\boldsymbol{i}^*(k-1) + 4\boldsymbol{i}^*(k-1) - \boldsymbol{i}^*(k-3) \tag{5}$$

Table I shows the 16 possible output voltage vectors generated by the four-leg VSI, depending on the switching states, where the '*p*' and '*n*' states of each leg implies that the upper and the lower switch of the corresponding leg is in the On state. Table I also indicates that the load current at the $(k+1)^{th}$ step in (4) can be predicted according to the voltage vector determined by the 16 switching states. Among the 16 possibilities for the future load current at the $(k+1)^{th}$ step, an optimal predicted current that can minimize the error between the reference and predicted load currents can be decided by the cost function given by (6). Note that the three-phase four-leg VSI requires 16 repeated calculations to find the optimal switching state resulting in the optimal predicted current. If the [*pppp*] state or the [*nnnn*] state is selected because of the cost function, the switching state should be determined by considering the switching loss. For example, in case the present switching state is [*ppnp*], and the [*pppp*] state or the [*nnnn*] state is selected as a result of the cost function, [*pppp*] should be used at the $(k+1)^{th}$ step to reduce the number of phases involved with the commutation.

$$g = \left|\boldsymbol{i}^*(k+1) - \boldsymbol{i}(k+1)\right| \tag{6}$$

The overall block diagram of the conventional model predictive current control method for the three-phase four-leg VSI is shown in Fig. 2.

III. Proposed Model Predictive Control Method

The cost function of the conventional model predictive control method for the load current control of the four-leg VSI is based on the load current error, which compares the reference and actual load currents to select the future optimum switching state, as shown in (6). Moreover, the future optimum switching state can be determined by the VSI voltage shown in Table I. In the load current dynamics of the four-leg VSI expressed as (4), one can assume that the one-step future load currents become equal to the one-step future current references by applying the voltage reference. As a result, the load current dynamics in (4) can be written as,

$$\boldsymbol{v}^*(k) = R\boldsymbol{i}(k) + \frac{L}{T_s}\left[\boldsymbol{i}^*(k+1) - \boldsymbol{i}(k)\right] \tag{7}$$

The reference voltage vector can be assessed by a cost function defined as,

TABLE I
THE POSSIBLE SWITCHING STATES AND THE CORRESPONDING OUTPUT PHASE VOLTAGES OF THE FOUR-LEG INVERTER

Switching states	Output phase voltage			Switching states	Output phase voltage		
	v_{an}	v_{bn}	v_{cn}		v_{an}	v_{bn}	v_{cn}
pppp	**0**	**0**	**0**	***pppn***	V_{dc}	V_{dc}	V_{dc}
nnnp	$-V_{dc}$	$-V_{dc}$	$-V_{dc}$	***nnnn***	**0**	**0**	**0**
pnnp	**0**	$-V_{dc}$	$-V_{dc}$	***pnnn***	V_{dc}	**0**	**0**
ppnp	**0**	**0**	$-V_{dc}$	***ppnn***	V_{dc}	V_{dc}	**0**
npnp	$-V_{dc}$	**0**	$-V_{dc}$	***npnn***	**0**	V_{dc}	**0**
nppp	$-V_{dc}$	**0**	**0**	***nppn***	**0**	V_{dc}	V_{dc}
nnpp	$-V_{dc}$	$-V_{dc}$	**0**	***nnpn***	**0**	**0**	V_{dc}
pnpp	**0**	$-V_{dc}$	**0**	***pnpn***	V_{dc}	**0**	V_{dc}

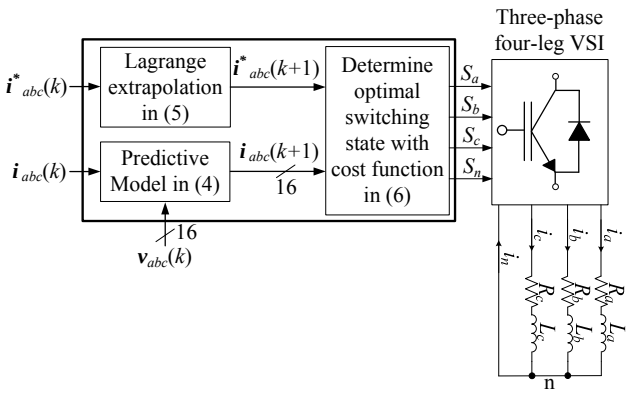

Fig. 2. Block diagram of the conventional model predictive control method for the three-phase four-leg VSI.

$$g = \left| \mathbf{v}^*(k) - \mathbf{v}(k) \right| \tag{8}$$

Equation (8) implies that the voltage vector closest to the reference voltage vector, among the 16 possible voltage vectors of the four-leg VSI, generates the optimal switching state. The 16 voltage vectors of the four-leg VSI in the *abc* coordinate depicted in Table I, can be transformed into the *αβγ* coordinate by the *abc* to *αβγ* transformation in (9).

$$T = \frac{2}{3}\begin{bmatrix} 1 & -\frac{1}{2} & -\frac{1}{2} \\ 0 & \frac{\sqrt{3}}{2} & -\frac{\sqrt{3}}{2} \\ \frac{1}{2} & \frac{1}{2} & \frac{1}{2} \end{bmatrix} \tag{9}$$

The resultant components of the voltage vectors expressed in the *αβγ* coordinate are illustrated in Table II. In addition, the vector diagram with the voltage vectors expressed in the *αβγ* coordinate is shown in Fig. 3. The six sectors on the *αβ* plane can be defined by projecting the prisms in the *αβγ* coordinate on the *αβ* plane, as shown in Fig. 3. The resultant projection on the *αβ* plane of the 16 voltage vectors of the three-phase four-leg VSI is the same as the 2D space vectors of the three-phase three-leg inverter. Assuming that the reference voltage vector of the three-phase four-leg VSI is located in Fig. 3, the switching state to generate the voltage vector closest to the reference voltage vector is the [*pnnn*] state, as shown in Fig. 3. As a result, the [*pnnn*] state should be selected as the optimal switching state to minimize the voltage error between the reference and VSI voltage vectors. This implies that an optimal voltage vector can be directly selected if the voltage vector closest to the reference voltage vector among the 16 voltage vectors of the three-phase four-leg VSI can be determined at every sampling period.

Fig. 4 illustrates that each prism is divided into four tetrahedrons. For example, if the reference voltage vector is located in tetrahedron 1.1 as shown in Fig. 4, the switching state to generate the voltage vector nearest to the reference voltage vector becomes one among the [*pppp*], [*nnnn*], [*pnnn*], [*pnnp*], and [*ppnp*] states. The polarities in parentheses shown in Fig. 4 are the polarities of each phase voltage of the three-phase four-leg VSI in the tetrahedron. The optimal switching state can be selected by determining the voltage vector closest to the reference voltage vector.

This paper proposes a model predictive control method based on a vector preselection technique for the three-phase four-leg VSI to find the voltage vector closest to the reference voltage vector. This method determines the position of the reference voltage at every sampling instant. Based on the position of the reference voltage, three active voltage vectors surrounding the reference voltage vector can be preselected among the entire 14 active voltage vectors generated by the three-phase four-leg VSI, as shown in Fig. 4. In addition to the three preselected active voltage vectors, two zero vectors corresponding to the switching states, [*pppp*] and [*nnnn*], are included as optimal voltage vector candidates. As a result, only five vectors surrounding the reference voltage vector can be judged as candidates for the optimal voltage vector based on the position of the reference voltage vector at every sampling period, without considering all the 16 voltage vectors generated by the three-phase four-leg VSI. Thus, the calculation burden for determining the optimal voltage vector closest to the reference voltage vector can be reduced from 16 to 5 calculations. As a result, the proposed method can demonstrate the same performance as the conventional model predictive control method with reduced calculation burden.

In order to preselect five voltage vectors near the reference voltage vector during every sampling period, the 3D space in

TABLE II
PHASE VOLTAGES IN THE ABΓ COORDINATE SYSTEM CORRESPONDING TO ALL THE SWITCHING STATES

Switching states	Phase voltage in $\alpha\beta\gamma$ coordinate			Switching states	Phase voltage in $\alpha\beta\gamma$ coordinate		
	v_α	v_β	v_γ		v_α	v_β	v_γ
pppp	0	0	0	*pppn*	0	0	V_{dc}
nnnp	0	0	$-V_{dc}$	*nnnn*	0	0	0
pnnp	$\frac{2}{3}V_{dc}$	0	$-\frac{2}{3}V_{dc}$	*pnnn*	$\frac{2}{3}V_{dc}$	0	$\frac{1}{3}V_{dc}$
ppnp	$\frac{1}{3}V_{dc}$	$\frac{1}{\sqrt{3}}V_{dc}$	$-\frac{1}{3}V_{dc}$	*ppnn*	$\frac{1}{3}V_{dc}$	$\frac{1}{\sqrt{3}}V_{dc}$	$\frac{2}{3}V_{dc}$
npnp	$-\frac{1}{3}V_{dc}$	$\frac{1}{\sqrt{3}}V_{dc}$	$-\frac{2}{3}V_{dc}$	*npnn*	$-\frac{1}{3}V_{dc}$	$\frac{1}{\sqrt{3}}V_{dc}$	$\frac{1}{3}V_{dc}$
nppp	$-\frac{2}{3}V_{dc}$	0	$-\frac{1}{3}V_{dc}$	*nppn*	$-\frac{2}{3}V_{dc}$	0	$\frac{2}{3}V_{dc}$
nnpp	$-\frac{1}{3}V_{dc}$	$-\frac{1}{\sqrt{3}}V_{dc}$	$-\frac{2}{3}V_{dc}$	*nnpn*	$-\frac{1}{3}V_{dc}$	$-\frac{1}{\sqrt{3}}V_{dc}$	$\frac{1}{3}V_{dc}$
pnpp	$\frac{1}{3}V_{dc}$	$-\frac{1}{\sqrt{3}}V_{dc}$	$-\frac{1}{3}V_{dc}$	*pnpn*	$\frac{1}{3}V_{dc}$	$-\frac{1}{\sqrt{3}}V_{dc}$	$\frac{2}{3}V_{dc}$

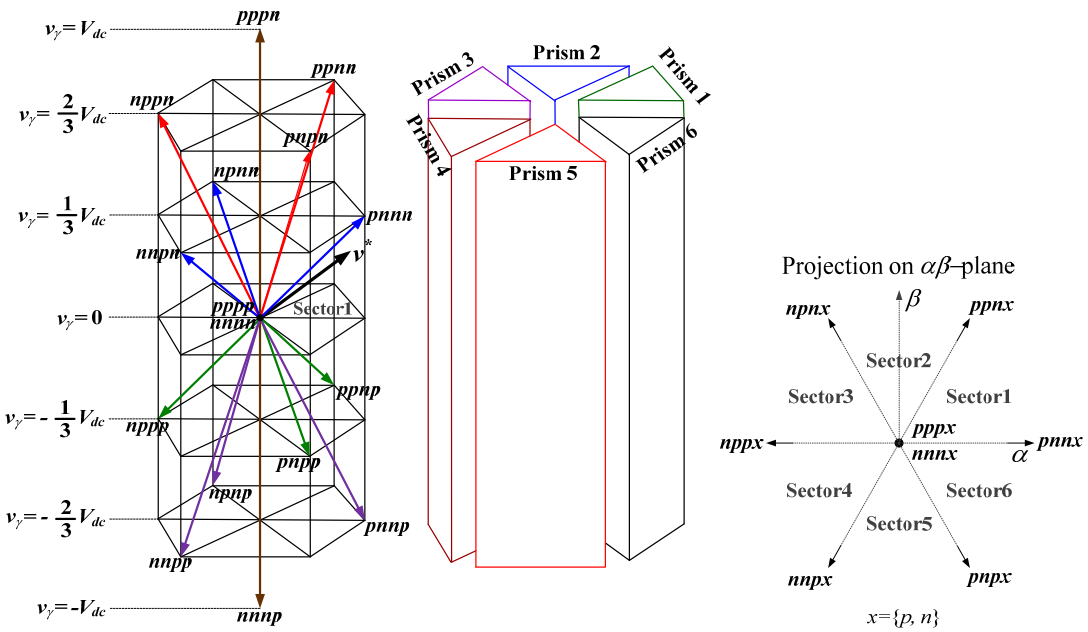

Fig. 3. 3-dimensional space vectors and prisms in $\alpha\beta\gamma$ coordinate and the projection result of the 3-dimensional space vectors on the $\alpha\beta$ plane.

the $\alpha\beta\gamma$ coordinate can be divided into 24 tetrahedrons because each prism contains four tetrahedrons. For example, prism 1 includes four tetrahedrons from tetrahedron 1.1 to 1.4, as shown in Fig. 4. Each tetrahedron has five voltage vectors, in which two are zero voltage vectors, whereas the other three are nonzero voltage vectors. The two zero vectors correspond to the switching states, [*pppp*] and [*nnnn*]. Furthermore, Fig.4 shows that the three nonzero voltage vectors contain the polarity information of the three output phase voltages of the three-phase four-leg VSI. Therefore, the four tetrahedrons can be identified with the polarities of the three output phase voltages. This finding implies that once the polarities of the three output phase voltages are determined at every sampling period, the tetrahedron, where the reference voltage vector is located, can be identified, as shown in Fig. 4. As a result, three active voltage vectors of the three-phase four-leg VSI can be preselected after the sector and the tetrahedron are known at every sampling period. The sector is determined by projecting the reference voltage vector expressed in the $\alpha\beta\gamma$ coordinate on $\alpha\beta$-plane. Moreover, the tetrahedron is decided by the polarities of each phase voltage of the reference voltage vector represented in the *abc* frame. The optimal voltage vector closest to the reference voltage vector can be selected by the cost function in (8) among the three preselected active vectors and the two zero vectors only. For instance, assume that the reference voltage vector projected on the $\alpha\beta$-plane in the $\alpha\beta\gamma$ coordinate is located in sector 1 and the three-phase output phase voltages of the reference

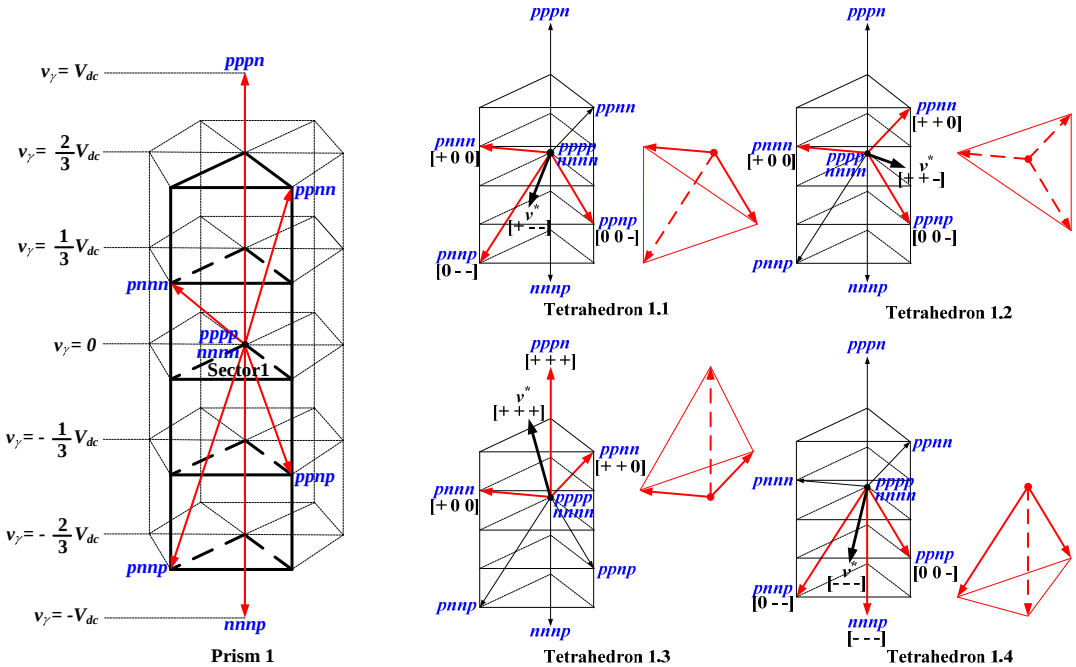

Fig. 4. Example of the vector preselection technique with the reference voltage vector in Prism 1.

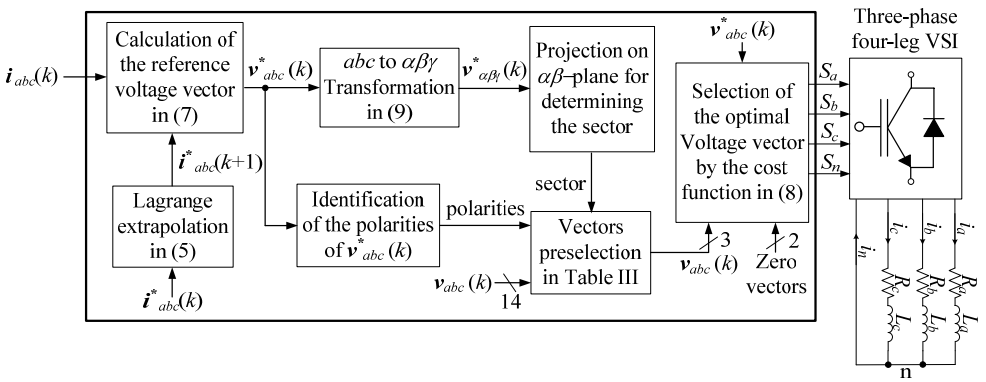

Fig. 5. Block diagram of the proposed method.

voltage vector in the *abc* frame are $v^*_{an} \geq 0$, $v^*_{bn} \leq 0$, and $v^*_{cn} \leq 0$. Given that the reference voltage vector is located in tetrahedron 1.1, the three active voltage vectors corresponding to the switching state - [*pnnn*], [*pnnp*], and [*ppnp*] - are preselected. These three active vectors and the two zero vectors are evaluated relative to cost function to select one optimal voltage vector. The three nonzero switching states and the two zero states for the preselected vectors in the 24 tetrahedrons are summarized in Table III. Therefore, once the position of the reference voltage vector is determined, the five preselected voltage vectors are directly selected as candidates for the optimal voltage vector. The block diagram of the proposed model predictive control method based on the vector preselection technique is shown in Fig. 5. Note that if the zero voltage vector is selected as the optimal vector, the switching state with less switching commutations in consideration of the previous switching state is used between the [*pppp*] and [*nnnn*] states.

Equation (7) is based on the backward difference method derived by the discrete-time modeling of the load current dynamics in (4); this is accomplished by assuming that the one-step future load currents become equal to the one-step future current references by applying the voltage reference. A more sophisticated discrete-time modeling for reference voltage production can be obtained by discretization based on a more sophisticated method, instead of approximation according to a backward finite-difference method. For the continuous-time state model in (10) and the derivative of the state variable in (11), the discrete-time state-space equation can be represented as (12).

$$\dot{\mathbf{x}}(t) = \mathbf{A}\mathbf{x}(t) + \mathbf{B}\mathbf{u}(t) \tag{10}$$

$$\dot{\mathbf{x}}(t) = \lim_{T_s \to 0} \frac{\mathbf{x}(t+T_s) - \mathbf{x}(t)}{T_s} \tag{11}$$

$$\mathbf{x}((k+1)T_s) = (\mathbf{I} + T_s\mathbf{A})\,\mathbf{x}(kT_s) + T_s\mathbf{B}\mathbf{u}(kT_s) \tag{12}$$

TABLE III
PRESELECTED SWITCHING STATES IN THE 24 TETRAHEDRONS OF THE THREE-PHASE FOUR-LEG VSI

Location of $v^*_{\alpha\beta\gamma}(k)$	Projection result	Polarities of $v^*_{abc}(k)$	Preselected switching states
Tetrahedron 1.1 in prism 1	Sector 1	[+ - -]	*pppp nnnn pnnn pnnp ppnp*
Tetrahedron 1.2 in prism 1		[+ + -]	*pppp nnnn pnnn ppnn ppnp*
Tetrahedron 1.3 in prism 1		[+ + +]	*pppp nnnn pnnn ppnn pppn*
Tetrahedron 1.4 in prism 1		[- - -]	*pppp nnnn pnnp ppnp nnnp*
Tetrahedron 2.1 in prism 2	Sector 2	[+ + -]	*pppp nnnn ppnn ppnp npnn*
Tetrahedron 2.2 in prism 2		[- + -]	*pppp nnnn ppnp npnn npnp*
Tetrahedron 2.3 in prism 2		[+ + +]	*pppp nnnn ppnn npnn pppn*
Tetrahedron 2.4 in prism 2		[- - -]	*pppp nnnn ppnp npnp nnnp*
Tetrahedron 3.1 in prism 3	Sector 3	[- + -]	*pppp nnnn npnn npnp nppp*
Tetrahedron 3.2 in prism 3		[- + +]	*pppp nnnn npnn nppn nppp*
Tetrahedron 3.3 in prism 3		[+ + +]	*pppp nnnn npnn nppn pppn*
Tetrahedron 3.4 in prism 3		[- - -]	*pppp nnnn npnp nppp nnnp*
Tetrahedron 4.1 in prism 4	Sector 4	[- + +]	*pppp nnnn nppn nppp nnpn*
Tetrahedron 4.2 in prism 4		[- - +]	*pppp nnnn nppp nnpn nnpp*
Tetrahedron 4.3 in prism 4		[+ + +]	*pppp nnnn nppn nnpn pppn*
Tetrahedron 4.4 in prism 4		[- - -]	*pppp nnnn nppp nnpp nnnp*
Tetrahedron 5.1 in prism 5	Sector 5	[- - +]	*pppp nnnn nnpn nnpp pnpp*
Tetrahedron 5.2 in prism 5		[+ - +]	*pppp nnnn nnpn pnpn pnpp*
Tetrahedron 5.3 in prism 5		[+ + +]	*pppp nnnn nnpn pnpn pppn*
Tetrahedron 5.4 in prism 5		[- - -]	*pppp nnnn nnpp pnpp nnnp*
Tetrahedron 6.1 in prism 6	Sector 6	[+ - +]	*pppp nnnn pnpn pnpp pnnn*
Tetrahedron 6.2 in prism 6		[+ - -]	*pppp nnnn pnpp pnnn pnnp*
Tetrahedron 6.3 in prism 6		[+ + +]	*pppp nnnn pnpn pnnn pppn*
Tetrahedron 6.4 in prism 6		[- - -]	*pppp nnnn pnpp pnnp nnnp*

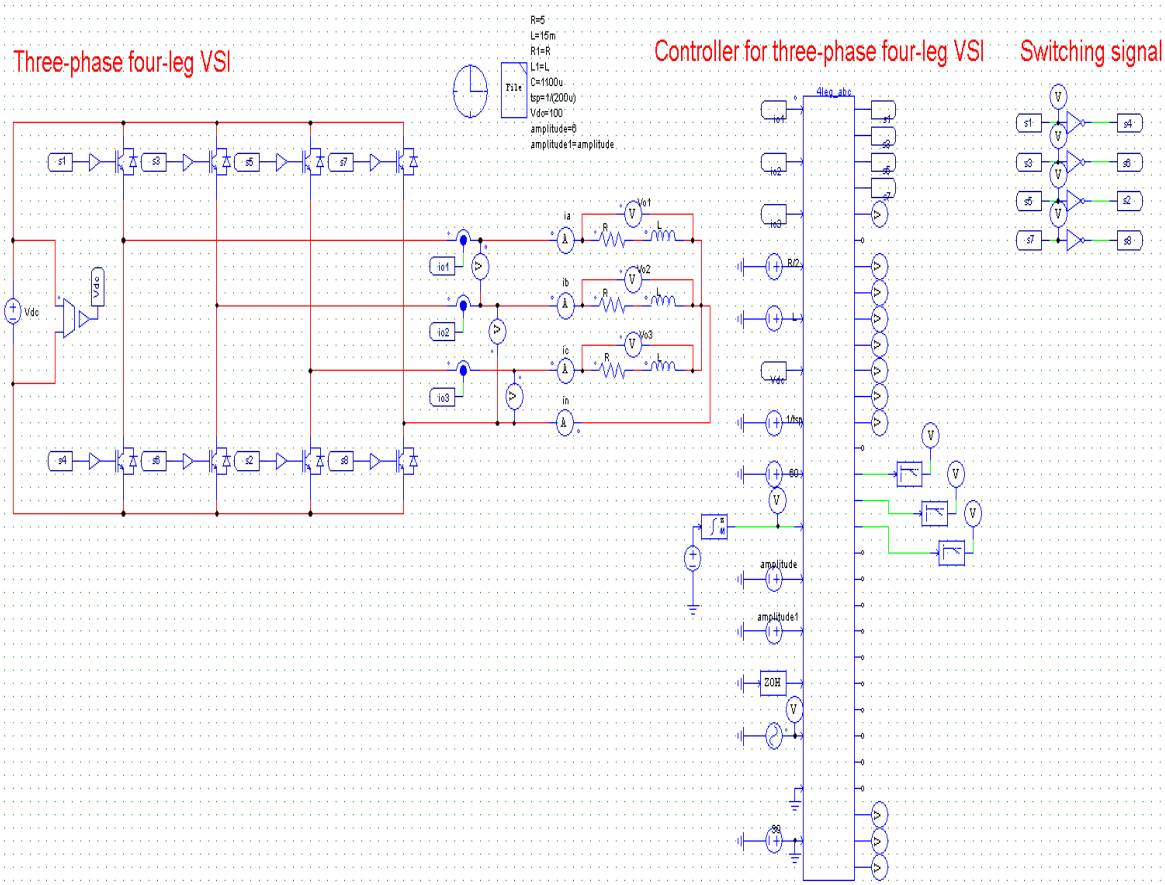

Fig. 6. PSIM schematic figure used in the simulation.

In a discrete-time domain where the input variables change value only at discrete-time instants kT_s, the state equation based on exact discrete-time model can be written by

$$\boldsymbol{x}(k+1)=\mathbf{A}_{\mathbf{d}}\boldsymbol{x}(k)+\mathbf{B}_{\mathbf{d}}\boldsymbol{u}(k) \tag{13}$$

where, $\mathbf{A}_{\mathbf{d}}=e^{\mathbf{A}T_s}$ and $\mathbf{B}_{\mathbf{d}}=\left(\int_0^T e^{\mathbf{A}\tau}d\tau\right)\mathbf{B}$.

The load current dynamics of the four-leg inverter in (2) can be expressed as

$$\dot{\boldsymbol{i}}(t)=\frac{d\boldsymbol{i}}{dt}=\mathbf{A}\boldsymbol{i}(t)+\mathbf{B}\boldsymbol{u}(t) \tag{14}$$

where, $\mathbf{A}=-\frac{R}{L}$, $\mathbf{B}=\frac{1}{L}$, $\boldsymbol{u}(t)=\boldsymbol{v}(t)$

Therefore, the load current dynamics of the inverter, expressed in the discrete-time domain with the discrete-time state-space equations, is

$$\boldsymbol{i}(k+1)=\mathbf{A}_{\mathbf{d}}\boldsymbol{i}(k)+\mathbf{B}_{\mathbf{d}}\boldsymbol{u}(k) \tag{15}$$

where, $\mathbf{A}_{\mathbf{d}}=e^{\mathbf{A}T_S}$,

$$\mathbf{B}_{\mathbf{d}}=\left(\int_0^T e^{\mathbf{A}\tau}d\tau\right)\mathbf{B}=\mathbf{A}^{-1}(\mathbf{A}_d-\mathbf{I})\mathbf{B}=-\frac{1}{R}\left(e^{-\frac{RT_S}{L}}-1\right),$$

$\boldsymbol{u}(k)=\boldsymbol{v}(k)$

Based on the exact discrete-time model, the load current dynamics with the discrete-time state-equation can be more precisely written in the discrete-time domain as

$$\boldsymbol{i}(k+1)=e^{-\frac{RT_S}{L}}\boldsymbol{i}(k)-\frac{1}{R}\left(e^{-\frac{RT_S}{L}}-1\right)\boldsymbol{v}(k) \tag{16}$$

With assumption that the one-step future load currents become equal to the one-step future current references through the voltage reference application, the reference voltage vector can be expressed as

$$\boldsymbol{v}^*(k)=\left\{\frac{e^{-\frac{RT_S}{L}}}{\left(e^{-\frac{RT_S}{L}}-1\right)/\mathrm{R}}\right\}\boldsymbol{i}(k)-\left\{\frac{1}{\left(e^{-\frac{RT_S}{L}}-1\right)/\mathrm{R}}\right\}\boldsymbol{i}^*(k+1)+\boldsymbol{e}(k) \tag{17}$$

Owing to the fast sampling and the switching frequency of the inverter in this paper, the discrete-time modeling based on the finite-difference method in (7), which is simpler in (17), can be simply implemented in this paper.

IV. Simulation and Experiment Results

To demonstrate the effectiveness of the proposed method, a simulation was carried out using PSIM during steady-state, and transient-state with balanced and unbalanced loads. The PSIM schematic figure in Fig. 6 shows the implementation of the proposed model predictive control algorithm in a

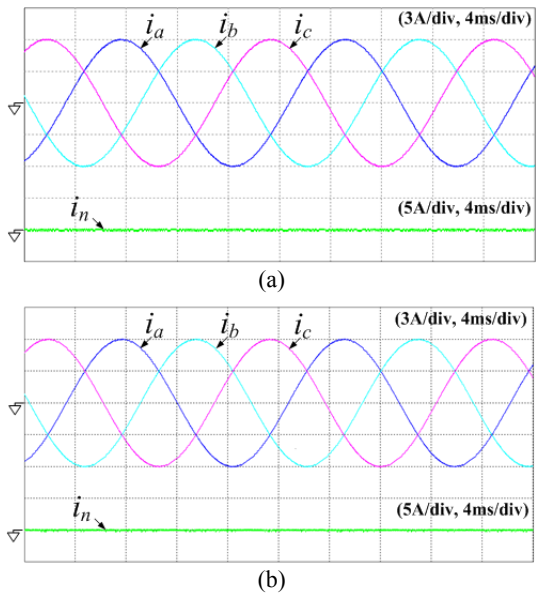

Fig. 7. Simulation results of the load and neutral currents (i_a, i_b, i_c, i_n) with T_s = 20 μs, a balanced load, and balanced references (i^*_a = i^*_b = i^*_c = 6 A at 60 Hz) for (a) the proposed method, (b) the conventional method.

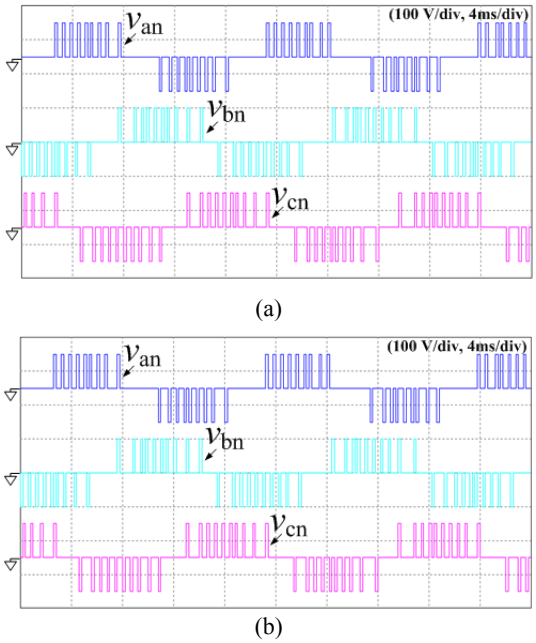

Fig. 8. Simulation results of each phase voltage with T_s = 200μs for (a) the proposed method and (b) the conventional method.

simplified C-block with programming. Figs. 7 (a) and (b) show the simulation results of the load currents and the neutral current during steady-state of the conventional and proposed methods, respectively, with T_s = 20μs, V_{dc} = 100V, C = 2200μF, a balanced load (R_a = R_b = R_c = 2.5Ω, L_a = L_b = L_c = 15mH), and balanced references (i^*_a = i^*_b = i^*_c = 6A at 60Hz). Furthermore, Figs. 7 (a) and (b) demonstrate that the load currents of both methods track their references well, and the neutral current is zero because of the balanced references. In addition, the simulation results of the proposed method exhibits the same performance as the conventional method, such as a total harmonic distortion (THD) value of 0.7%.

To clarify the argument that the proposed method has the same performance as the conventional method, the simulation results of each phase voltage during the steady-state of both methods with T_s = 200 μs, a balanced load (R_a = R_b = R_c = 2.5 Ω, L_a = L_b = L_c = 15 mH), and balanced references (i^*_a = i^*_b = i^*_c = 6A at 60 Hz) are shown in Figs. 8 (a) and (b), respectively. Note that from the Figs. 8 (a) and (b), the simulation result of the proposed method is exactly the same as the conventional method result. This finding indicates that the proposed method performs similarly as the conventional method because the switching states of both methods are the same at every sampling instant. Thus, only the results of the proposed method can be shown.

In Fig. 9, the simulation result of the load and neutral currents during the steady-state of the proposed method are presented with T_s = 20 μs, a balanced load (R_a = R_b = R_c = 2.5 Ω, L_a = L_b = L_c = 15 mH), and unbalanced references (i^*_a = 6 A at 60 Hz, i^*_b = i^*_c = 3 A at 30 Hz). This simulation is carried out to demonstrate the effectiveness of the proposed

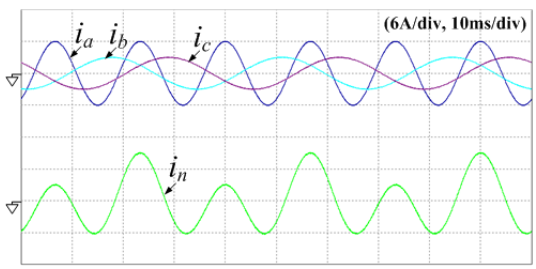

Fig. 9. Simulation results of the load and neutral currents (i_a, i_b, i_c, i_n) in the proposed method with T_s = 20 μs, a balanced load and unbalanced references (i^*_a = 6 A at 60 Hz, i^*_b = i^*_c = 3 A at 30 Hz).

method under different demands in each phase of the load based on typical applications of the three-phase four-wire systems. The load currents track their references well with minimal steady-state error and the neutral current is equal to the sum of the three-phase currents. In addition, Fig. 10 shows the simulation results of the load currents and the neutral current during the steady-state of the proposed method with T_s = 20 μs, an unbalanced load (R_a = R_b = 2.5 Ω, L_a = L_b = 15 mH, phase-c has no load), and unbalanced references (i^*_a = 6 A at 60 Hz, i^*_b = 3 A at 30 Hz, i^*_c = 0). Similar to the case of the balanced load and unbalanced references, the load and neutral currents flow with minimal steady-state error. Furthermore, the result when an open-circuit fault in phase-c occurs can be known because the current reference in phase-c should be set to zero by a fault detection algorithm [18].

In Figs. 11 and 12, the dynamic responses during transient-state of the proposed method are shown with T_s = 20μs, a balanced load (R_a = R_b = R_c = 2.5 Ω, L_a = L_b = L_c = 15 mH),

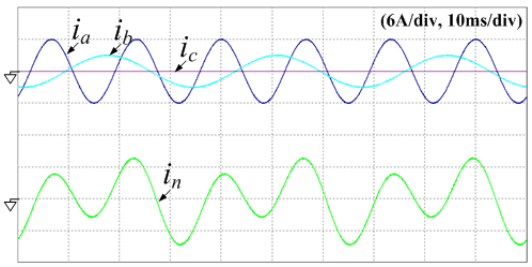

Fig. 10. Simulation results of the load and neutral currents (i_a, i_b, i_c, i_n) in the proposed method with T_s = 20 μs, an unbalanced load (phase-c has no load) and unbalanced references (i^*_a = 6 A at 60 Hz, i^*_b = 3 A at 30 Hz, i^*_c = 0).

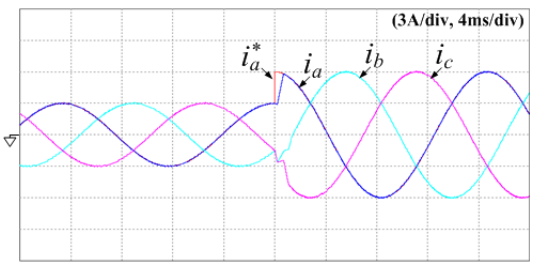

Fig. 11. Simulation results of the load currents (i_a, i_b, i_c) and the phase-a reference (i^*_a) with T_s = 20μs, a step change from 3 to 6 A, and a balanced load for the proposed method.

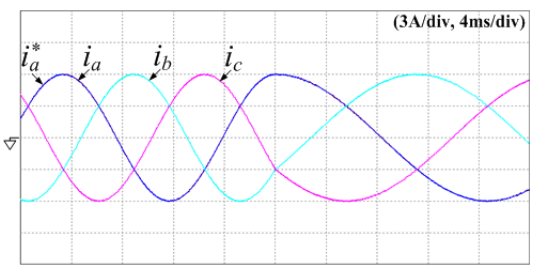

Fig. 12. Simulation results of the load currents (i_a, i_b, i_c) and the phase-a reference (i^*_a) with T_s = 20 μs, a step change from 60 to 30 Hz, and a balanced load for the proposed method.

and a balanced step change of the references. Figs. 11 and 12 show balanced double- and half-step changes in the magnitude and frequency commands of the references, respectively. Fig. 13 exhibits a half-step change of the phase-a reference under different demands on each phase of the load. Figs.11 to 13 exhibit that during transient-state, the load currents track well their references with rapid dynamics.

The simplified model predictive control method based on a future reference voltage vector was tested with a prototype setup of a three-phase four-leg VSI during steady-state and transient-state with balanced and unbalanced loads. A photo of the experimental setup is illustrated in Fig. 14. The setup consisted of a four-leg VSI with IGBT modules (SKM50GB123D), a SEMIKRON gate drivers (SKHI22A), a dc-link capacitor with V_{dc} = 100 V, and a Texas Instrument digital signal processor (DSP) board (TMS320F28335) with RL loads. The sampling frequency used in the simulation and the experiment was 50 kHz. In addition, a simple RC low-

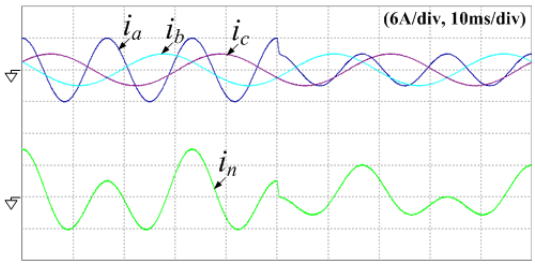

Fig. 13. Simulation results of the load and neutral currents (i_a, i_b, i_c, i_n) under different demands on each phase of the load with T_s = 20 μs, a step change of the phase-a reference from 6 to 3 A, and a balanced load for the proposed method.

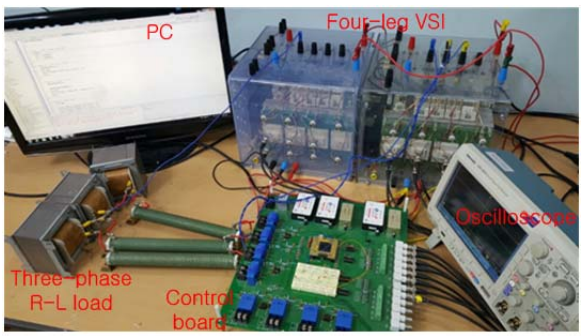

Fig. 14. A photo of the experimental setup.

pass filter was used in the input port of the ADC in the Texas Instrument DSP board (TMS320F28335) to reduce the noise effect. Figs. 15(a) and (b) show the experimental results of the load and neutral currents during the steady-state of the proposed and the conventional methods, respectively, with T_s = 20μs, V_{dc} = 100V, C = 2200 μF, a balanced load (R_a = R_b = R_c = 2.5 Ω, L_a = L_b = L_c = 15 mH), and balanced references (i^*_a = i^*_b = i^*_c = 6 A at 60 Hz). Similar to the simulation results, the load currents of both methods track their references well, and the neutral current is zero because of the balanced references. Furthermore, the same results demonstrate that the performance of the proposed method is the same as the conventional method.

The simulation results are presented to support that the proposed method has the same performance as the conventional method, as shown in Fig. 8. Fig. 16 presents the experimental results of each phase voltage during steady-state of both methods under the same conditions as the simulation. The proposed method indicates the same output phase voltages at every sampling instant as the conventional method, observed through the experimental results of both methods. Thus, only the experimental results of the proposed method in connection with the simulation results can be presented.

Fig. 17 shows the experimental results of the load and neutral currents during steady-state of the proposed method with T_s = 20 μs, a balanced load (R_a = R_b = R_c = 2.5 Ω, L_a = L_b = L_c = 15 mH), and unbalanced references (i^*_a = 6 A at 60 Hz, i^*_b = i^*_c = 3 A at 30 Hz). Furthermore, Fig. 18 presents the experimental results of the load and neutral currents

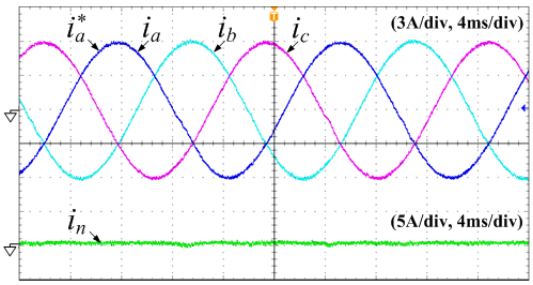

(a)

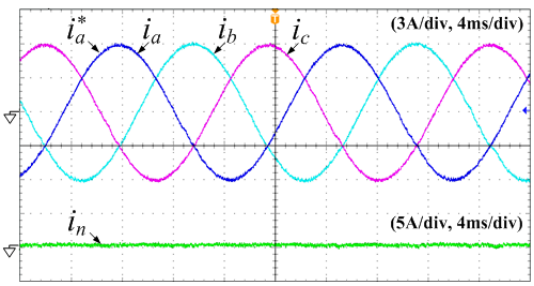

(b)

Fig. 15. Experimental results of the load and neutral currents (i_a, i_b, i_c, i_n) with T_s = 20 μs, a balanced load and balanced references ($i^*_a = i^*_b = i^*_c$ = 6 A at 60 Hz) for (a) the proposed method, (b) the conventional method.

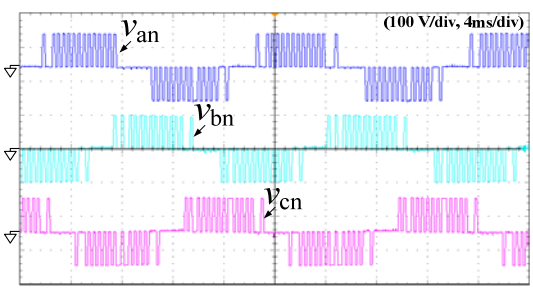

(a)

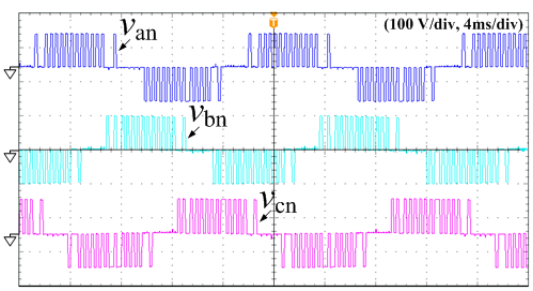

(b)

Fig. 16. Experimental results of each phase voltage with T_s = 200 μs for (a) the proposed method and (b) the conventional method.

during the steady-state of the proposed method with T_s = 20 μs, an unbalanced load ($R_a = R_b$ = 2.5 Ω, $L_a = L_b$ = 15 mH, phase-c has no load), and unbalanced references (i^*_a = 6 A at 60 Hz, i^*_b = 3 A at 30 Hz, i^*_c = 0). We can observe from Figs. 17 and 18 that the load and neutral currents flow with minimal steady-state error under different demands on each phase of the load.

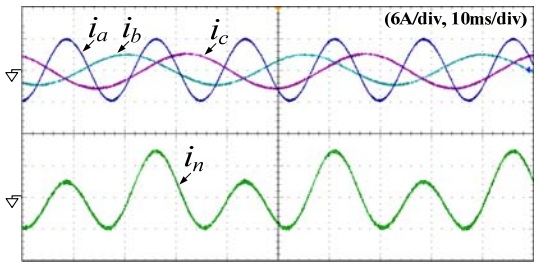

Fig. 17. Experimental results of the load and neutral currents (i_a, i_b, i_c, i_n) in the proposed method with T_s = 20 μs, a balanced load, and unbalanced references (i^*_a = 6 A at 60 Hz, $i^*_b = i^*_c$ = 3 A at 30 Hz).

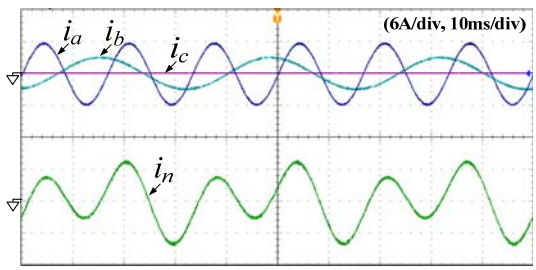

Fig. 18. Experimental results of the load and neutral currents (i_a, i_b, i_c, i_n) in the proposed method with T_s = 20 μs, an unbalanced load (phase-c has no load), and unbalanced references (i^*_a = 6 A at 60 Hz, i^*_b = 3 A at 30 Hz, i^*_c = 0).

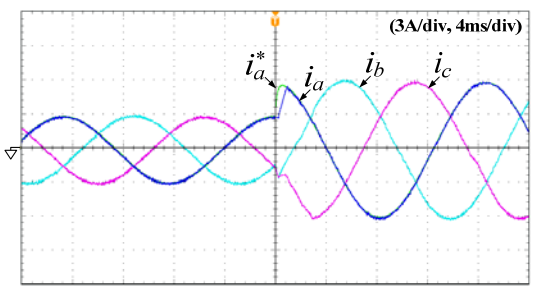

Fig. 19. Experimental results of the load currents (i_a, i_b, i_c) and the phase-a reference (i^*_a) with T_s = 20 μs, a step change from 3 to 6 A, and a balanced load for the proposed method.

Figs. 19 to 21 exhibit the experimental results of the proposed method for the analysis of the dynamic responses during transient-state by setting a step change in the controllers with T_s = 20 μs and a balanced load ($R_a = R_b = R_c$ = 2.5 Ω, $L_a = L_b = L_c$ = 15 mH). Balanced double- and half-step changes in the magnitude and frequency command of the references are observed in Figs. 19 and 20, respectively. Moreover, the half-step change of the phase-a reference under different demands on each phase of the load is depicted in Fig. 21. In all three cases, the simplified model predictive control method during transient-state shows fast dynamic responses in common with the conventional method.

The model predictive control method is influenced by the accuracy of the parameters used for the control algorithm. Thus, Fig. 22 shows the effectiveness with the parameter errors in the control algorithms of both proposed and conventional methods. The effectiveness is verified through the THD value with T_s = 20 μs. The actual resistance value is

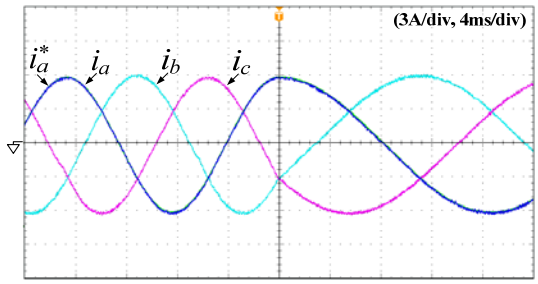

Fig. 20. Experimental results of the load currents (i_a, i_b, i_c) and the phase-a reference (i^*_a) with T_s = 20 μs, a step change from 60 to 30 Hz, and a balanced load for the proposed method.

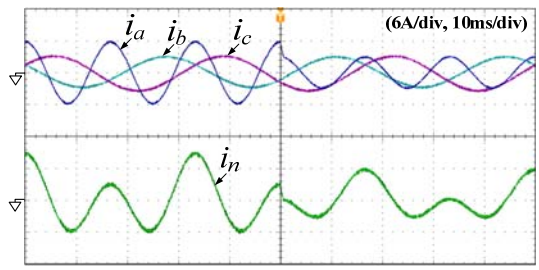

Fig. 21. Experimental results of the load and neutral currents (i_a, i_b, i_c, i_n) under different demands on each phase of the load with T_s = 20 μs, a step change of phase-a reference from 6 to 3 A, and a balanced load for the proposed method.

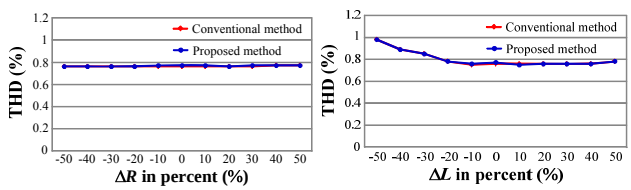

(a) (b)

Fig. 22. Simulation results with the parameter errors in the controllers with T_s = 20 μs for (a) the variations of the resistance and (b) the inductance.

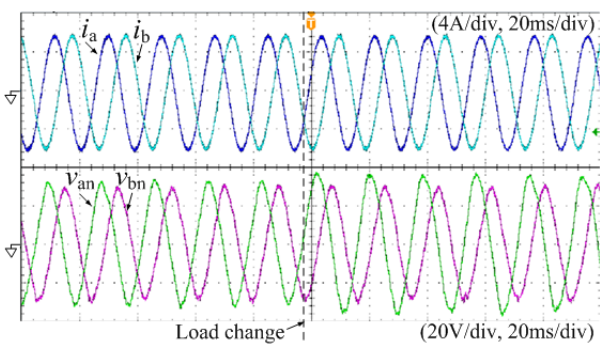

Fig. 23. Experimental results with load change in which the *a*-phase resistance has a step-change from 2.5 to 5 Ω as the *b*- and *c*-phase resistances maintain the 2.5 Ω (a) load currents and (b) filtered load phase voltages.

set to 2.5 Ω, whereas, the actual inductance value is 15 mH. The parameter variations used in the controllers are changed from -50% to 50% of the actual values. The errors of the resistance value in the controllers have a negligible effect on the THD values of both methods. However, when an inductance value is smaller than the actual value used in the controllers, the THD values in both methods increased. Although the proposed technique depends on the future reference voltage vector for the three-phase four-leg VSI, the dependency of the model accuracy on the performance is the same as that of the conventional method.

Experimental waveforms for the load currents and the filtered output phase voltages with load disturbance are shown in Fig. 23, in which the *a*-phase resistance has a step-change from 2.5 to 5 Ω as the *b*- and *c*-phase resistances are kept at 2.5 Ω. Note that the proposed method for the four-leg VSI can regulate the load current without disturbance even after a load change in one phase as shown in Fig. 23. The filtered *a*-phase load voltage in Fig. 23 increases according to the decreased load condition, whereas the filtered *b*-phase load voltage remains unchanged.

V. CONCLUSIONS

This paper proposes a simplified model predictive control method based on a future reference voltage vector for a three-phase four-leg VSI. The proposed technique can preselect three active voltage vectors among the entire 14 possible active voltage vectors produced by the three-phase four-leg VSI based on the position of the future reference voltage vector. The discrete-time model of the future reference voltage vector is established to predict the future movement of the load currents, and its position is used to choose three preselected active vectors at every sampling period. As a result, the proposed method can reduce calculation load by decreasing the candidate voltage vectors used in the cost function for the four-leg VSIs, while exhibiting the same performance as the conventional method. The effectiveness of the proposed method is demonstrated with simulation and experiment results.

ACKNOWLEDGMENT

This research was supported by the National Research Foundation of Korea (NRF) grant funded by the Korea government (MSIP) (2014R1A2A2A01006684), the Human Resources Development (No.20154030200860) of the Korea Institute of Energy Technology Evaluation and Planning (KETEP) grant funded by the Korea government Ministry of Trade, Industry and Energy, and the Chung-Ang University Excellent Student Scholarship.

REFERENCES

[1] M. Ryan, R. Lorenz, and R. De Doncker, "Modeling of multi-leg sine-wave inverters: A geometric approach," *IEEE Trans. Ind. Electron.*, Vol. 46, No. 6, pp. 1183-1191, Dec. 1999.

[2] J. Huang, R. Xiong, Z. Wang, W. Zuo, Y. Zhou, and H.

Shi, "A novel SPWM control strategy to reduce common-mode voltage in three-phase four-leg inverters," in *Proc. IEEE ICEMS Conf.*, Wuhan, China, Oct. 2008, pp. 1526-1530.
[3] J.-H. Kim and S.-K. Sul, "A carrier-based PWM method for three-phase four-leg voltage source converters," *IEEE Trans. Power Electron.*, Vol. 19, No. 1, pp. 66-75, Jan. 2004.
[4] J.-H. Kim, S.-K. Sul, and P. N. Enjeti, "A carrier-based PWM method with optimal switching sequence for a multilevel four-leg voltage-source inverter," *IEEE Trans. Ind. Appl.*, Vol. 44, No. 4, pp. 1239-1248, Jul. 2008.
[5] Y. Kumsuwan, W. Srirattanawichaikul, S. Premrudeepreechacharn, K. Higuchi, and H. Toliyat, "A carrier-based unbalanced PWM method for four-leg voltage source inverter fed asymmetrical two-phase induction motor," in *Proc. IEEE IPEC Conf.*, Singapore, Jun. 2010, pp. 2469-2476.
[6] N.-Y. Dai, M.-C.Wong, F. Ng, andY.-D.Han, "A FPGA-based generalized pulse width modulator for three-leg center-split and four-leg voltage source inverters," *IEEE Trans. Power Electron.*, Vol. 23, No. 3, pp. 1472-1484, May 2008.
[7] D. Shen and P. Lehn, "Fixed-frequency space-vector-modulation control for three-phase four-leg active power filters," *IEE Proc. Electr. Power Appl.*, Vol. 149, No. 4, pp. 268-274, Jul. 2002.
[8] S. L. Salazar, H. F. Zapata, and F. E.Weichmann, "Analysis, design and experimental evaluation of a four-pole PWM rectifier using space vector modulation," in *Proc. IEEE-PESC'97 Conf.*, 1997, pp. 484-490.
[9] R. Zhang, V. Prasad, D. Boroyevich, and F. Lee, "Three-dimensional space vector modulation for four-leg voltage-source converters," *IEEE Trans. Power Electron.*, Vol. 17, No. 3, pp. 314-326, May 2002.
[10] M. Zhang, D. J. Atkinson, B. Ji, M. Armstrong, and M. Ma, "A near state three dimensional space vector modulation for a three phase four leg voltage source inverter," *IEEE Trans. Power Electron.*, Vol. 29, No. 11, pp. 5715-5726, Nov. 2014.
[11] J. Rodriguez, J. Pontt, C. A. Silva, P. Correa, P. Lezana, P. Cortes, and U. Ammann, "Predictive current control of a voltage source inverter," *IEEE Trans. Ind. Electron.*, Vol. 54, No. 1, pp. 495-503, Feb. 2007.
[12] S. Moon and S. Kwak, "Reducing Common-Mode Voltage of Three-Phase VSIs with Predictive Current Control Method without Cost Function," *Journal of Power Electronics*, Vol. 15, No. 3, pp. 712-720, May 2015.
[13] S. Kwak and J. Park, "Predictive Control Method with Future Zero-Sequence Voltage to Reduce Switching Losses in Three-Phase Voltage Source Inverters," *IEEE Transactions on Power Electronics*, Vol. 30, No. 3, pp. 1558-1566, Mar. 2015.
[14] V. Yaramasu, M. Rivera, B. Wu, and J. Rodriguez, "Model predictive current control of two-level four-leg inverters-part I : concept, algorithm and simulation analysis," *IEEE Trans. Power Electron.*, Vol. 28, No. 7, pp. 3459-3468, Jul. 2013.
[15] P. Cortes, J. Rodriguez, C. Silva, and A. Flores, "Delay compensation in model predictive current control of a three-phase inverter," *IEEE Trans. Ind. Electron.*, Vol. 59, No. 2, pp. 1323-1325, Feb. 2012.
[16] A. Ziani, A. Llor, and M. Fadel, "Model predictive current controller for four-leg converters under unbalanced conditions," in *Proc. IEEE Eur. Conf. Power Electron. and Appl.*, pp. 1-10, 2011.
[17] M. Rivera, V. Yaramasu, A. Llor, J. Rodriguez, B. Wu, and M. Fadel, "Digital predictive current control of a three-phase four-leg inverter," *IEEE Trans. Ind. Electron.*, Vol. 60, No. 11, pp. 4903-4912, Nov. 2013.
[18] R. L. A. Riberio, C. B. Jacobina, E. R. C. da Silva, and A. M. N. Lima, "Fault-tolerant voltage-fed PWM inverter AC motor drive systems," *IEEE Trans. Ind. Electron.*, Vol. 51, No. 2, pp. 439-446, Apr. 2004.

Soo-eon Kim received his B.S. degree in Electrical and Electronics Engineering from Chung-ang University, Seoul, Korea in 2014, where he is currently working toward his M.S degree in Electrical and Electronics Engineering. His research interests are analysis and control for voltage source inverters and active front ends.

So-Young Park received the B.S. degree in Electrical and Electronics Engineering from Chung-ang University, Seoul, Korea in 2014, where he is currently working toward his M.S degree in Electrical and Electronics engineering. His research interests include modulation method and control algorithm for ac/dc and dc/ac converters.

Sangshin Kwak (S'02-M'05) received the Ph.D. degree in Electrical Engineering from Texas A&M University, College Station, Texas in 2005. From 1999 to 2000, he worked as a research engineer at LG Electronics, Changwon, Korea. He was also with Whirlpool R&D Center, Benton Harbor, MI, in 2004. From 2005 to 2007, he worked as a Senior Engineer in Samsung SDI R&D Center, Yongin, Korea. From 2007 to 2010, he worked as an assistant professor at Daegu University, Gyeongsan, Korea. Since 2010, he has been with Chung-ang University, Seoul, Korea, currently as an associate professor. His research interests are topology design, modeling, control, and analysis of ac/dc, dc/ac, ac/ac power converters including resonant converters for adjustable speed drives and digital display drivers, as well as modern control theory applied to DSP-based power electronics.